

University of Windsor

## Scholarship at UWindsor

---

Mechanical, Automotive & Materials  
Engineering Publications

Department of Mechanical, Automotive &  
Materials Engineering

---

9-1-2023

# Thermal modelling of a passive style net-zero greenhouse in Alberta: The effect of ground parameters and the solar to air fraction

Oselen J. Imafidon  
*University of Windsor*

David S.K. Ting  
*University of Windsor*

Rupp Carriveau  
*University of Windsor*

Follow this and additional works at: <https://scholar.uwindsor.ca/mechanicalengpub>



Part of the [Automotive Engineering Commons](#), and the [Mechanical Engineering Commons](#)

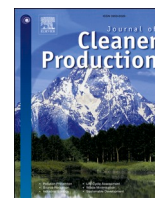
---

### Recommended Citation

Imafidon, Oselen J.; Ting, David S.K.; and Carriveau, Rupp. (2023). Thermal modelling of a passive style net-zero greenhouse in Alberta: The effect of ground parameters and the solar to air fraction. *Journal of Cleaner Production*, 416.

<https://scholar.uwindsor.ca/mechanicalengpub/43>

This Article is brought to you for free and open access by the Department of Mechanical, Automotive & Materials Engineering at Scholarship at UWindsor. It has been accepted for inclusion in Mechanical, Automotive & Materials Engineering Publications by an authorized administrator of Scholarship at UWindsor. For more information, please contact [scholarship@uwindsor.ca](mailto:scholarship@uwindsor.ca).



# Thermal modelling of a passive style net-zero greenhouse in Alberta: The effect of ground parameters and the solar to air fraction

Oselen J. Imafidon, David S-K. Ting, Rupp Carriveau\*

*Turbulence and Energy Laboratory, University of Windsor, 401 Sunset Ave, Windsor, ON, Canada*

## ARTICLE INFO

Handling Editor: Panos Seferlis

## ABSTRACT

Agricultural greenhouses can provide a suitable microclimate for crops to thrive under extreme weather conditions. The operations of these greenhouses are expensive due to the energy requirement of the active thermal conditioning systems required to maintain the growing environment for crop production. Engineering of these greenhouses to utilize clean renewable energy sources is critical and necessary to mitigate their carbon footprint, paving the way to a more sustainable agricultural industry. This paper presents numerical modelling of a net-zero passive solar greenhouse in Alberta, Canada with winter temperatures below freezing. The indoor microclimate of the greenhouse is modelled using the detailed radiation model of a transient simulation tool, TRNSYS. The paper investigates the effects of ground parameters and the solar-to-air fraction on the numerical results. The paper includes a cost comparison between crop production in the traditional and passive style greenhouse.

## 1. Introduction

The connection between national food security and climate-resilient growing environments continues to be reinforced with each force majeure that devastates another field agricultural operation. Controlled environment agriculture (CEA) helps to insulate production from the extreme outdoor climate. The irony in this is that this often requires significant energy to achieve, energy conversion that can actually contribute to climate change itself.

The climate of Canada with the exception of part of the West coast, has a severely cold winter season characterized by average temperatures below freezing (Britannica, 2019). The growing season is short, making it impossible to meet all season's vegetable needs without importation and or the use of controlled greenhouses (Dias et al., 2017). Currently, the operation of these controlled greenhouses is the most energy-intensive sector of agriculture (Mazzeo et al., 2021). The Independent Electricity System Operator (IESO) report shows the electricity demand of the greenhouse sector in the province of Ontario as one of the fastest growing commercial sectors (IESO, 2019). The problem is worse for the remote communities in Canada's subarctic, accessible only by air and water during the summer and has higher energy prices due to the absence of connection to the grid (Henshaw, 2017).

Conventional greenhouses require active systems for indoor climate

conditioning which contribute to their high energy demands. The heating demand of these greenhouses' accounts for 70–80% of the energy requirement (Cuce et al., 2016). Research has produced numerous energy savings technologies and strategies to be sustainable with some including renewables to be useful in reducing the energy consumption of conventional-style greenhouses (Cuce et al., 2016). However, given the massive energy demands of these commercial (often artificially lit) greenhouses, they must have significant supplemental sources that include the grid connection and/or onsite fossil power generation. On the other hand, select traditional “Chinese-Style” greenhouses can operate passively without any additional energy requirement in Northern China. These greenhouses are widely utilized for vegetable growing in Northern China even in the coldest winter months when the monthly daily average temperature falls below  $-10\text{ }^{\circ}\text{C}$  (Tong et al., 2013) and play a critical role in ensuring food security.

The Chinese-style greenhouses (CSGs) utilize the abundant clean energy from the sun to meet the thermal energy required for the growth of plants within the growing area enclosed by the greenhouse. The favourable growing microclimate of the CSGs is attributed to the orientation, heat storage medium and heat retention strategies incorporated in their design. The CSGs (see Fig. 1) are orientated East West for maximum exposure to solar radiation with a transparent South roof (mostly covered with a plastic layer), an opaque North roof made from

\* Corresponding author. Civil and Environmental Engineering, Environmental Energy Institute, Turbulence and Energy Laboratory, University of Windsor, Windsor, ON, N9B 3P4, Canada.

E-mail address: [rupp@uwindsor.ca](mailto:rupp@uwindsor.ca) (R. Carriveau).

<https://doi.org/10.1016/j.jclepro.2023.137840>

Received 6 April 2023; Received in revised form 24 May 2023; Accepted 16 June 2023

Available online 19 June 2023

0959-6526/Crown Copyright © 2023 Published by Elsevier Ltd. All rights reserved.

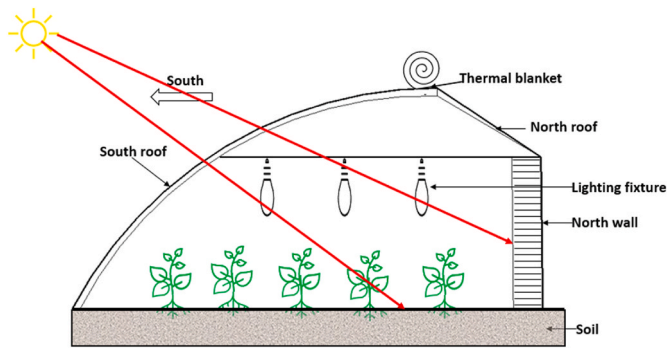


Fig. 1. Cross-sectional view of a Chinese-style greenhouse.

lightweight materials, an opaque North wall made from massive materials such as brick, clay, etc., opaque insulated East and West end walls and a thermal blanket for heat preservation purposes (Cao et al., 2019). The North wall is the main heat storage medium, and the thermal blanket is the heat retention medium. These greenhouses are being adopted outside of China in countries like Japan, Korea, and Russia (Gao et al., 2010) due to their excellent performance with the need for supplemental heating in some places in Canada (Beshada et al., 2006). Notably, the CSGs have been adopted by a grower in Alberta, Canada to grow vegetables in the cold winter season without supplemental heating requirements (Labby, 2021).

Several authors have performed experimental and numerical studies to comprehend the influence of the cross-sectional design parameters on

the utilization of solar energy in CSG. The effect of the structural properties of three different types of North walls was investigated by Wang et al. (2014). Their study conceptually divided the North wall from interior to exterior side into three layers with different functions; the heat storage layer, the thermal stable layer and the insulating layer, the study noted that reducing the North wall beyond a particular size eliminates the thermal stable layer. Liu et al. (Liu et al. 2020) studied the internal surface structure of the North wall's effect on the thermal microclimate of a CSG using four different surface structures: plane, vertical, horizontal and alveolate wall. The study found the heat storage capacity of the North wall to be influenced by its structure and the air temperature to be influenced by the accumulated heat load released by the wall with alveolate surface structure wall having the highest capacity for thermal accumulation Zhang et al. (2011) experimentally studied the heat absorption and release of walls and ground in a solar greenhouse in a sunny and cloudy day. The study concluded the heat energy released from the storage wall and ground depends on the solar radiation in the greenhouse. These studies were performed for solar greenhouses with a single (mono) South roof and the numerical tools codes are not available in the open.

In Canada, the adoption of the CSG is slow and not widespread due to several barriers thus the reported studies on the application of CSG in Canada are few. One such study was experimentally performed in Southern Manitoba, the study presented the winter performance of the CSG in the local area (Beshada et al., 2006). The key finding of the experiment was that solar radiation had the most influence on the greenhouse temperature profile. The research also found the average daily energy released by the North wall to be 4% less than its average

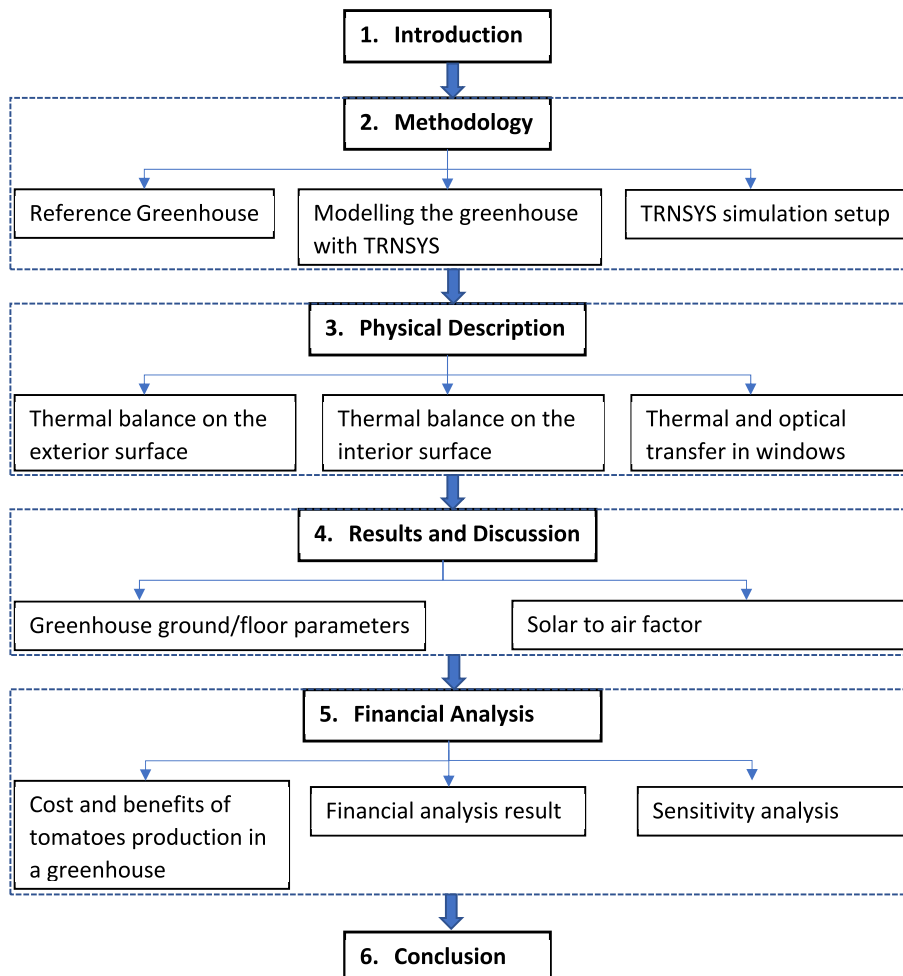


Fig. 2. Flowchart of the paper structure.



Fig. 3. Picture of the energy self-sufficient reference greenhouse in Olds, Alberta.

stored energy and a supplemental heating requirement to maintain the required greenhouse temperature. Dong et al. (2021) numerically modelled the energy performance of a conceptually CSG based on the local climate of Saskatoon and found that crop production in the CSG greenhouse could provide annual heating savings of 55% in comparison to the traditional greenhouses. In contrast to the reported studies on the thermal performance of CSG in Canada, a grower in the province of Alberta has adopted the CSG successfully operating without supplemental heating for multiple winter seasons (Labby, 2021). Although the ambient temperature in Alberta is low during the winter season, its solar potential is enormous ranking second in the amount of solar irradiation received amongst the provinces in Canada (Energyhub, 2021). An

average installed solar system can produce about 1276kWh of electricity per kW of solar panel per year almost as sunny as Rio de Janeiro, Brazil. The CSG greenhouse adopted by the grower is slightly different from the greenhouse in other reported studies in Canada as it has a double South roof configuration.

Accurate modelling and simulation of CSGs and conventional greenhouse growing environments are important to determine the influential components/parameters for thermal performance and for the optimization of operational energy consumption. It is also essential to better understand design material requirements and the potential for extending the growing season to ultimate year-round crop production. The development of thermal models that can predict the growing environment requires several assumptions to simplify the complex heat and mass transfer process to an acceptable fidelity. Some parameters of the model have been shown to have a significant effect on the energy requirement of the greenhouse. Zhang et al. (Zhang and Zou, 2013) showed the CSG to be more efficient in harnessing solar energy when the incidence angle was not fixed. The configuration of the North wall (thickness and material) has been shown to affect the interior microclimate of the CSGs (Liu et al., 2019; Wang et al., 2014).

Although the previous studies reported are limited to CSG with single South roofs, the findings reveal solar radiation to be an influential parameter to the performance of the passive solar greenhouse (Beshada et al., 2006; Zhang et al., 2011) In this paper, the energy-self-sufficient CSG having double South facing roof in Alberta is chosen as the reference greenhouse for our study. A dynamic simulation software Transient System Simulation (TRNSYS) is used to model the microclimate of the

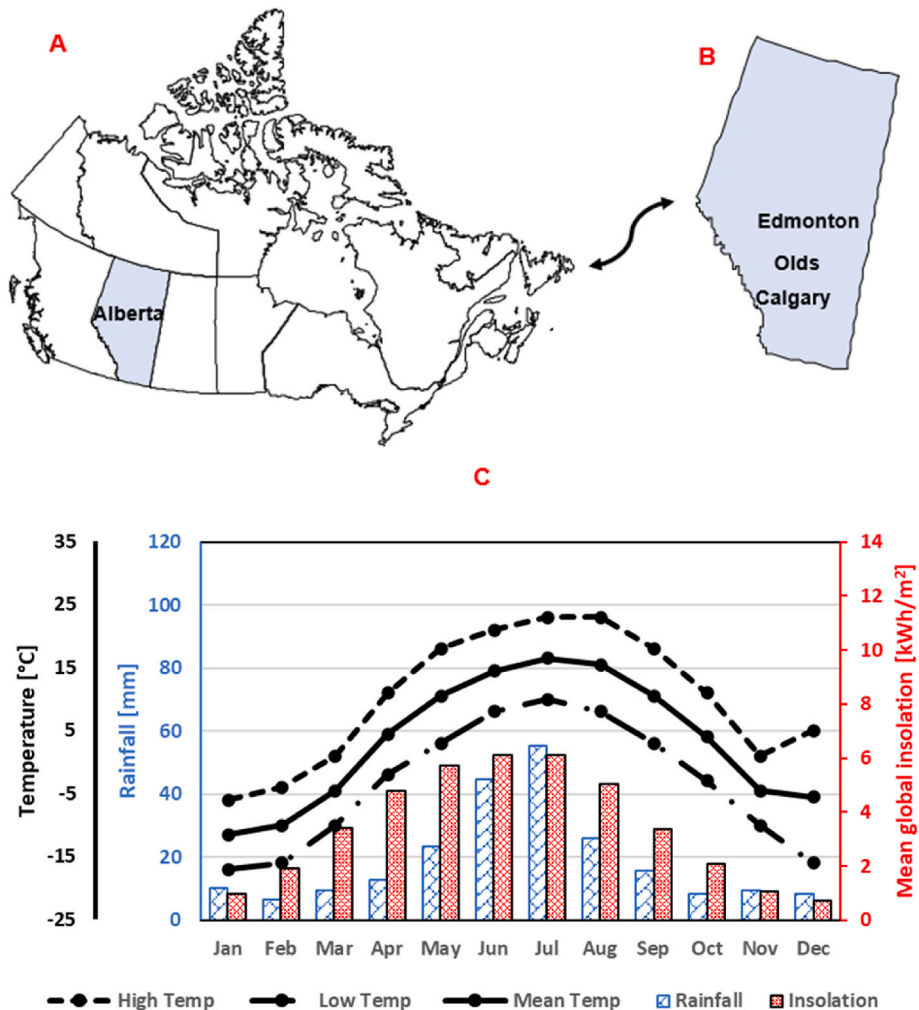


Fig. 4. Map of greenhouse location (Olds, Alberta, Canada) and climate parameters (Natural Resource Canada, 2020).

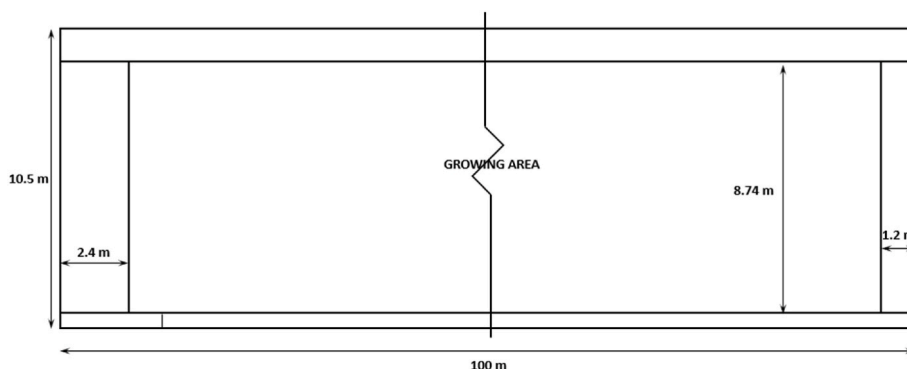


Fig. 5a. Plan view of the reference greenhouse.

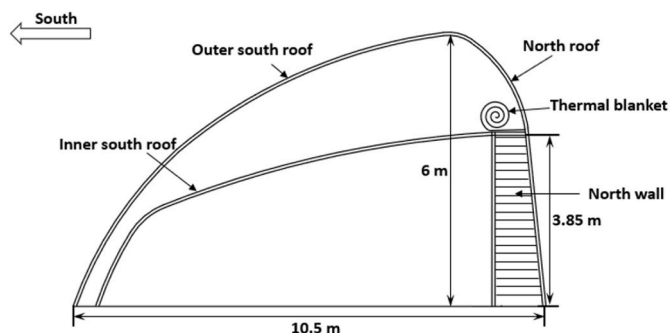


Fig. 5b. Cross-sectional view of the reference greenhouse.

greenhouse. TRNSYS is employed as the simulation tool detailed mode enables for more accurate modelling of the influence of solar radiation through the double South roof of the reference greenhouse. Certain assumptions are made to use this mode and a one-at-a-time approach is used to analyze the effect of parameters with high uncertainty. The parameters include the thickness of the soil layer, the soil temperature and the solar-to-air fraction. The paper also includes a financial analysis comparing the production in the traditional greenhouse and the CSG in Alberta using tomato production as a case study. The structure/development of the paper is depicted in Fig. 2. To the best of our knowledge, no paper has presented results on double South roof CSG in Canada and on the solar-to-air fraction on greenhouses.

## 2. Methodology

### 2.1. Reference greenhouse

The reference greenhouse (see Fig. 3) is constructed as a Chinese-style greenhouse by FreshPal Farms. It is located at Olds Alberta (latitude: 51.79 °N and longitude: 114.11 °W). The climate of Olds Alberta falls under the Dfb subtype of the Koppen Geiger climate classification having a warm summer and continental nature. The average temperature is low in the winter season with a mean monthly temperature of -11.5 °C in the coldest month but there is sufficient global solar insolation through the winter months as shown in Fig. 4.

The greenhouse structural framework is made of steel pipes, and it covers a floor area of 1050 m<sup>2</sup> (100 m X 10.5 m) with a growing area of 840 m<sup>2</sup> (96 m X 8.74 m) as illustrated in Fig. 5a. The greenhouse is oriented East-West with double curved roofs oriented South and covered with transparent polyolefin plastic to utilize solar energy in the winter season. The greenhouse operates passively in the winter season with no additional energy requirement for supplementary heating or cooling. The ridge heights of the greenhouse and its growing area measure 6 m and 3.85 m respectively as illustrated in Fig. 5b. The outer south-facing roof is a modification of the typical Chinese-style greenhouse based on the relatively heavy snow climate of Alberta.

The outer roof has a steeper curvature to reduce snow accumulation and snow vibrators are installed to aid the removal of excess snow. The inner south-facing roof is completely transparent during the hours of sunshine, and a movable thermal blanket (cotton material) covers it at night for heat preservation. The North roof is tapered towards the top, and it is filled with clay. The clay in this wall acts as a thermal storage medium for the greenhouse due to the thermal capacitance. It absorbs the solar thermal energy from the sun during the day and releases it at night passively. The East and West internal walls are insulated with Styrofoam and all other walls which form the building enclosure of the greenhouse are opaque. The description of the layers of the main greenhouse surfaces and wall construction is summarized in Table 1.

### 2.2. Modelling the greenhouse with TRNSYS

The dynamic heat and mass transfer exchanges in the greenhouse are modelled using Transient System Simulation Tool (TRNSYS). These processes are complex, and our dynamic modelling effort focused on the main exchanges critical to the performance of the greenhouse and are illustrated in Fig. 6 and are highlighted below.

1. The orientation of the greenhouse is East-West to utilize the energy from solar radiation, therefore the optical and thermal transmission through the south-facing transparent roofs is important. The division of the thermal model into zones was such that direct and diffuse shortwave radiation through the two South roofs reaches the growing area. The different options for zoning the model and the limitation of solar radiation treatment are discussed.

Table 1  
Wall materials for the surfaces of the reference greenhouse.

Surfaces	Materials (from outside to inside)
South roofs	Polyolefin plastic film (0.12 mm)
Inner south roof at night	Thermal blanket (25.4 mm) and PO plastic film (0.12 mm)
North roof	Thermal blanket (25.4 mm)
North wall	Thermal blanket (25.4 mm), Clay (609–914 mm) and Metal sheathing (36 mm)
East and West internal wall	Metal sheathing (36 mm), Styrofoam insulation (50.8 mm) and Metal sheathing (36 mm)
East and West external wall	Metal sheathing (36 mm)
Floor	Soil

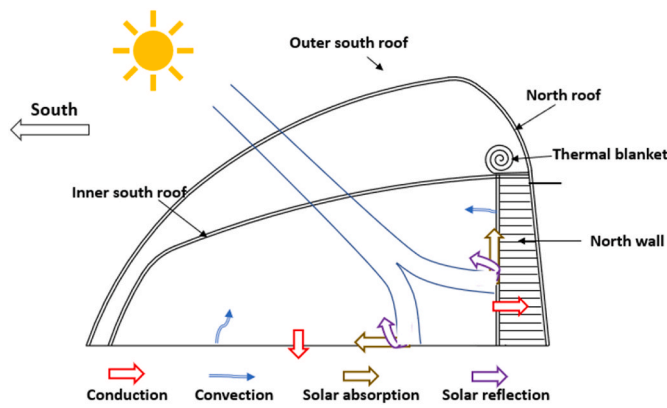


Fig. 6. Heat transfer process in the reference greenhouse.

2. The thermal storage and transfer through the North wall and ground of the greenhouse. The accurate distribution of solar radiation incident on these surfaces is important. The numerical tools mode used to study the distribution of shortwave radiation and infrared radiation between surfaces in a zone are discussed in Section 3 and were applied in our thermal model. The calibration of the ground parameters was one of our focuses in this work.
3. The fraction of beam and diffuse solar radiation into the growing area immediately converted to heat flux is studied. This is defined as the solar to air factor ( $f_{solair}$ ) in TRNSYS and can be set from 0 to 1, zero representing no immediate conversion of solar radiation to heat flux to the air and 1 signifying all the solar radiation is converted to heat flux to the air.

The three-dimensional model of the greenhouse (see Fig. 7) is drawn using Trnsys3D extension for Trimble SketchUp and is imported into TRNSYS for thermal simulation. The different thermal zones are assigned in SketchUp while creating the geometric model. TRNSYS allows for the treatment of shortwave and infrared radiation using either the standard mode or the detailed mode. The passage of beam shortwave radiation through internal windows between zones of more than two passages requires a detailed radiation mode. Using the simplified mode,



Fig. 7. Top view of the SketchUp 3D model of the reference greenhouse.

the beam radiation can not pass through the second internal window as it is treated as diffuse radiation after passing the second internal window (TRNSYS 18, 2021). Here we use a strategic technique to discretize the thermal stratification of a zone by using a fictive window which splits it into multiple air nodes to allow for beam solar radiation to pass through different thermal strata.

The detailed radiation model was used for our study as it was important for the beam and diffuse radiation to reach the growing area. The thermal zones must be closed volume, convex (i.e., all the internal angles of the zone should be less than  $180^\circ$ ) and should not intrude on other zones for the algorithm of the detailed radiation model to generate the required view factors matrices (TRNSYS 18, 2021). Various possibilities for partitioning the greenhouse exist that meaningfully represent thermal stratification considering the heat and mass transfer in the greenhouse. One option is dividing the thermal model into two thermal zones with the inner south roof and internal end walls as the boundaries. The limitation of this approach is the detailed model for the distribution of shortwave and longwave radiation can not be employed due to the concave geometry of the upper zone. The greenhouse could be divided into three zones with the middle zone having its convex and nonconvex sections separated by a virtual surface that permits shortwave radiation into the growing area. This approach removes the inner south roof surface and allows for view factors to be calculated but the limitation is that the view factor is calculated using the outer south roof only. A third option divides the greenhouse into three zones separated by the internal end walls with the outer south roof modelled as a double-glazed window with an approximate air gap. In this approach, the nonconvex area is approximated as a double-glazed window, the detailed radiation model can be invoked with the view factors matrix of the growing area formed using the inner surfaces. The third option was used for our modelling (see Fig. 7) as it allows the detailed radiation mode to be employed and the view factor of the growing area is based on the surfaces in the growing area. The limitation of this approach is the heat transfer process between the walls in the space above the inner South facing roof is not considered. The influence of solar radiation entering the growing area outweighs these heat transfer processes. Also, the effect of the solar-to-air factor in the growing area can only be specified and thus studied using this approach.

The geometric input data requires that windows are created as sub-surface of a wall and windows must be planar with straight line edges (Aschaber et al., 2009). The walls of the curved edges of the greenhouse south roof are simplified as four straight partitions with angles of  $173^\circ$ ,  $172^\circ$ ,  $175^\circ$  and  $140^\circ$  respectively and the windows are created by using an offset of 0.15 m. This offset is recommended to enable the program to generate the view factor matrix (TRNSYS-users Archives, 2023). The geometry of the south-facing roof covering the growing area has an overall windows surface of 88 %. The south roof's transparent covering is made of 4.8 mil polyolefin plastic (polyethylene) film. The optical and thermal properties of the glazing system of up to six

Table 2  
Glazing properties of double-layer polyethylene.

Glazing System Angular properties											
Angle	0	10	20	30	40	50	0.632	70	80	90	Hemis
$T_{sol}$	0.747	0.747	0.745	0.74	0.728	0.699	0.054	0.489	0.244	0	0.65
$Abs_1$	0.044	0.044	0.044	0.046	0.048	0.05	0.038	0.058	0.063	0	0.05
$Abs_2$	0.035	0.035	0.035	0.036	0.037	0.038	0.277	0.035	0.028	0	0.036
$R_{f_{sol}}$	0.175	0.175	0.175	0.178	0.187	0.213	0.277	0.417	0.664	1	0.254
$R_{b_{sol}}$	0.175	0.175	0.175	0.178	0.187	0.213	0.277	0.417	0.664	1	0.254
$T_{vis}$	0.747	0.747	0.745	0.74	0.728	0.699	0.632	0.489	0.244	1	0.65
$R_{f_{vis}}$	0.175	0.175	0.175	0.178	0.187	0.213	0.277	0.417	0.664	1	0.254
Glazing layer properties											
	$Emis_f$		$Emis_b$		Thickness (mm)		Conductance ( $W/m^2K$ )				
Glazing 1	0.79		0.79		0.1		3300				
Glazing 2	0.79		0.79		0.1		3300				

**Table 3**  
Thermophysical properties of wall construction materials.

Material	Conductivity W/m • K	Heat capacity J/kg • K	Density kg/m <sup>3</sup>	Resistance m <sup>2</sup> • K/W
Thermal blanket (Liu et al., 2019)	0.037	1600	70	-
Clay (TRNSYS 18, 2021)	0.869	1000	1800	-
Metal sheathing (TRNSYS 18, 2021)	-	-	-	2.4 × 10 <sup>-3</sup>
Styrofoam (TRNSYS 18, 2021)	0.031	1250	20	-
Soil (Ahamed et al., 2018)	1.400	1480	1975	-

glass panes required by TRNSYS for optical and thermal analysis are calculated using the Lawrence Berkeley National Lab Window program and the DOE2 file added to TRNSYS. The optical and angular values computed for a double-layer polyethylene material (Rasheed et al., 2018) and the properties used for the simulation are shown in Table 2 and the symbols are described in the nomenclature. The air gap with a thickness of 1.4 m is used to approximate the volume enclosed by the glazing system.

The North wall structural framing is tapered towards the top (see Fig. 5b) and filled with clay with a thickness of 609 and 914 mm. The interior East and West end walls are the boundary of the growing area of the greenhouse, and their wall construction is comprised of a Styrofoam insulation between two metal sidings. The exterior East and West facing walls is a layer of metal siding and the North roof is a layer of the thermal blanket. The floor area of the greenhouse is exposed to the soil. The thermophysical properties of the layers of the walls of the greenhouse are summarized in Table 3.

The ground/floor of the greenhouse is a dominant component for thermal transfer. The floor of the greenhouse is covered by soil. It is modelled as a boundary wall comprising a layer of soil of a specified depth having a constant outer boundary temperature. The ground temperature is relatively constant year-round and dependent on the location below an adequate depth which varies from 1 to 8 m for dry light soils or 20 m for moist heavy sandy soils (Kalogirou and Florides, 2004). Research has shown that during the winter season, short-period temperature fluctuation in ground temperature is prominent to a depth of 50 cm (Kalogirou and Florides, 2004). Soil temperature measurements at different depths in a similar greenhouse in Winnipeg Manitoba showed an almost constant temperature at a depth of 30 cm (Beshada et al., 2006). The effect of the deep ground depth and temperature are investigated in this study. The thermophysical properties of the soil layer are shown in Table 3.

The operation of the movable thermal blanket is controlled based on the availability of solar radiation and/or the interior temperature of the greenhouse. This feature of the greenhouse is not considered in this work as the precise control strategy employed during the period with available measurement was not recorded.

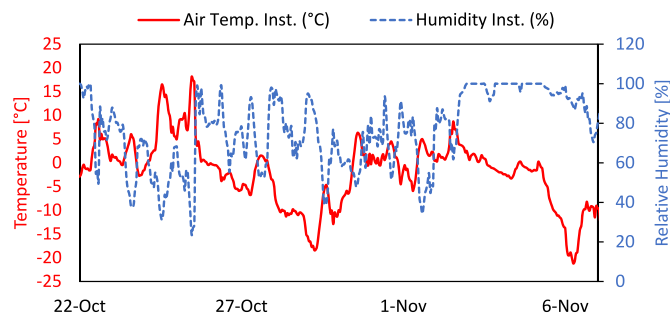


Fig. 8a. Ambient temperature and humidity.

2.3. TRNSYS simulation setup

The TRNSYS greenhouse model is calibrated against the measured temperature of the interior of the growing area of the greenhouse recorded between October 22 – November 7, 2019, in 15 min intervals. The exterior temperature, relative humidity, and global horizontal solar radiation for the period (see Fig. 8a and b) are retrieved from Alberta Agriculture, Forestry and Rural Economic Development (Alberta Climate Information Service, 2022).

The dewpoint temperature is calculated using the ambient temperature and relative humidity as described by Eq. (1) (1728 Software Systems, 2001).

$$T_{dp} = \frac{\left( 237.3 \times \left[ \frac{\ln\left(\frac{RH}{100}\right) + \left(\frac{17.27T_{amb}}{237.3 + T_{amb}}\right)}{17.27} \right] \right)}{\left( 1 - \left[ \frac{\ln\left(\frac{RH}{100}\right) + \left(\frac{17.27T_{amb}}{237.3 + T_{amb}}\right)}{17.27} \right] \right)} \tag{1}$$

The TRNSYS components setup is shown in Fig. 9. The data reader

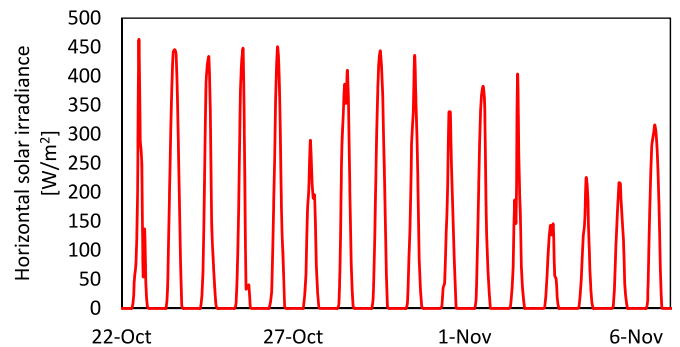


Fig. 8b. Horizontal solar irradiance.

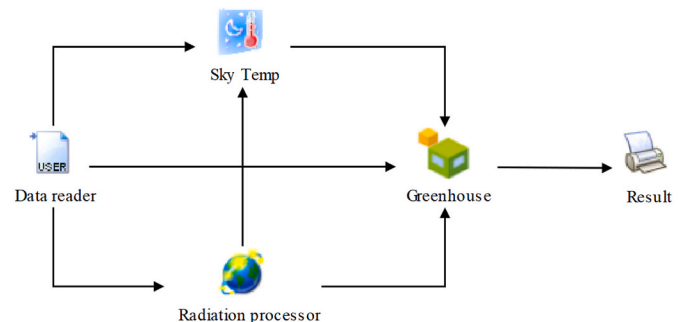


Fig. 9. TRNSYS simulation setup.

reads the supplied weather parameters and sends them to other components. The radiation processor estimates the radiation at the different greenhouse surfaces using the ambient temperature, relative humidity and global radiation on the horizontal. The surfaces are specified by their azimuth and slope angles. The sky temperature determines the effective sky temperature for longwave radiation exchange using a correlation between the ambient temperature and dewpoint temperature from the data reader and the beam radiation on the horizontal and diffuse radiation on the horizontal from the radiation processor. Type 56 model (greenhouse model) is fed its input from the data reader, radiation processor and sky temperature components and the simulation results are outputted to the printer component.

### 3. Physical description

This section describes the dynamic equation applied by TRNSYS to calculate the temperature of the greenhouse growing area. TRNSYS has a standard model and detailed model for calculating radiation (infrared, shortwave and point sources). The detailed model was applied in our work and its relevant equations are described below.

#### 3.1. Thermal balance on the exterior surface

The thermal energy balance at the exterior surfaces of the greenhouse is described using the equation below:

$$\dot{q}_{cv,o} + \dot{q}_{lw,o} + \dot{q}_{sol,o} = \dot{q}_{cd,o} \quad (2)$$

Here,  $\dot{q}_{cv,o}$  is the convective heat flux between the exterior side and its surrounding environment,  $\dot{q}_{lw,o}$  is the infrared radiation exchange between the exterior side and objects within its view,  $\dot{q}_{sol,o}$  is the shortwave radiation absorbed by the exterior side and  $\dot{q}_{cd,o}$  is the conductive heat transfer at the exterior side.

The convective heat flux depends on the exterior surface heat transfer coefficient  $h_o$  and the temperature difference between the exterior environment temperature  $T_{ext}$  and the exterior surface  $T_{s,o}$  as shown in the equation below.

$$\dot{q}_{cv,o} = h_o (T_{ext} - T_{s,o}) \quad (3)$$

The exterior heat transfer coefficient was set to 18 W/m<sup>2</sup>K for all wall surfaces with exception of the floor or ground. The exterior convective heat transfer coefficient of the ground was prescribed as  $2.8 \times 10^{-4}$  W/m<sup>2</sup>K which is recommended for surfaces with direct contact (TRNSYS 18, 2021). The exterior environment temperature is the ambient temperature for external walls, the temperature of the zone facing the external side for internal walls and the underground temperature for ground surface.

The shortwave radiation absorbed at the external surface is a function of solar absorptivity of the outer surface,  $\alpha_{sol,o}$  and the beam, diffuse and reflected solar radiation on the external surface,  $G_b$ ,  $G_d$  and  $G_r$  described by Eq. (4).

$$\dot{q}_{sol,o} = \alpha_{sol,o} (G_b + G_d + G_r) \quad (4)$$

The longwave radiation between the exterior side of the external walls and object within its view (sky and ground) is computed using Eq. (5) based on its view factor with the sky,  $F_{sky}$  and ground  $(1 - F_{sky})$  using a fictitious sky temperature,  $T_{fsky}$ .

$$\dot{q}_{lw,o} = \varepsilon_{s,o} \sigma (T_{fsky}^4 - T_{s,o}^4) \quad (5)$$

Here,  $\varepsilon_{s,o}$  is the emissivity to infrared radiation and  $\sigma$  is the Stefan Boltzmann constant. The fictitious sky temperature is a weighted temperature of the sky  $T_{sky}$  and ground  $T_{grd}$  described below and the net long radiation is described below.

$$T_{fsky} = (1 - F_{sky}) T_{grd} - F_{sky} T_{sky} \quad (6)$$

The dynamic conductive heat transfer at the exterior side  $\dot{q}_{cd,o}$  is computed using the transfer function method by Mitalas and Stephenson (TRNSYS 18, 2021). It is a function of the present and past values of the conduction heat flux on the outside surface temperature as described below.

$$\dot{q}_{cd,o} = \sum_{h=0}^{n_{a_s}} a_s^h T_{s,o}^h - \sum_{h=0}^{n_{b_s}} b_s^h T_{s,i}^h - \sum_{h=0}^{n_{d_s}} d_s^h \dot{q}_{cd,o}^h \quad (7)$$

The coefficients  $a_s$ ,  $b_s$  and  $d_s$  are the transfer functions for the current and past computed using the z-transfer function algorithm, and the superscript  $h$  represents the term in the time series (i.e., 0 refers to the current time, 1 refers to the past time and so on). The time series is calculated based on a time step referred to as time base.

#### 3.2. Thermal balance on the interior surface

The thermal energy balance at the interior surfaces is described by

$$\dot{q}_{cv,i} + \dot{q}_{lw,i} + \dot{q}_{sol,i} = -\dot{q}_{cd,i} \quad (8)$$

Here,  $\dot{q}_{cv,i}$  is the convective heat flux from the interior side to the zone air,  $\dot{q}_{lw,i}$  is the net infrared radiation with the surfaces within the zone,  $\dot{q}_{sol,i}$  represents the solar radiation transmitted through windows absorbed at the internal surface and  $\dot{q}_{cd,i}$  is the conduction heat flux at the interior surface.

The convective heat flux at the interior surface  $\dot{q}_{cv,i}$  is proportional to the interior surface heat transfer coefficient and the difference between the zone temperature  $T_{zone}$  and interior surface temperature  $T_{s,i}$ . The interior convective heat flux of 3 W/m<sup>2</sup>K was specified for all interior vertical surfaces.

$$\dot{q}_{cv,i} = h_i (T_{zone} - T_{s,i}) \quad (9)$$

The infrared radiation between the internal surfaces is calculated using the Gebhart method. This method assumes all surfaces have a constant temperature, emissivity and absorptivity that are independent of wavelength and direction (diffuse grey), opaque for infrared radiation with a constant hemispherical infrared reflectivity (TRNSYS 18, 2021). In this method, the infrared radiation that reaches and gets absorbed by a surface from another surface accounts for all possible paths and multiple reflections using the Gebhart factor. The matrix for the net infrared radiation  $\dot{Q}_{lw}$  in an enclosed zone can be expressed as

$$\dot{Q}_{lw} = (I - G_{lw}^T) A \varepsilon_{lw} \sigma T^4 \quad (10)$$

Here,  $I$  is the identity matrix,  $G_{lw}^T$  is the transpose of the Gebhart matrix for longwave radiation,  $A$  is the diagonal matrix of surface area in the enclosed zone,  $\varepsilon_{lw}$  is the emissivity and  $T$  is the vector of surface temperature. The Gebhart matrix is calculated from the emissivity, reflectivity  $\rho_{lw}$  and view factor matrix  $F$  as shown in the equation below.

$$G_{lw} = (I - F \rho_{lw})^{-1} F \varepsilon_{lw} \quad (11)$$

A fraction of the solar radiation transmitted through the windows can be specified to be immediately transferred as convective heat gain to the air using a solar-to-air factor  $f_{solair}$  with the remaining fraction distributed amongst the surfaces in the zone. The detailed direct shortwave radiation treatment is implemented using a so-called insolation matrix which contains the primary distribution of beam radiation through the external window. The insolation matrix is calculated by an integrated tool, TRNSHED and is made up of the sunlit fractions of the window that strike each inside surface of the zone for all patches of the celestial hemisphere. In this manner, the actual sun position can be used to select the matrix row in each simulation time step. The diffused solar radiation is distributed using a so-called solar Gebhart factor which represents the fraction of transmitted radiation through a surface that reaches another surface, and it is not reflected. The factor includes all

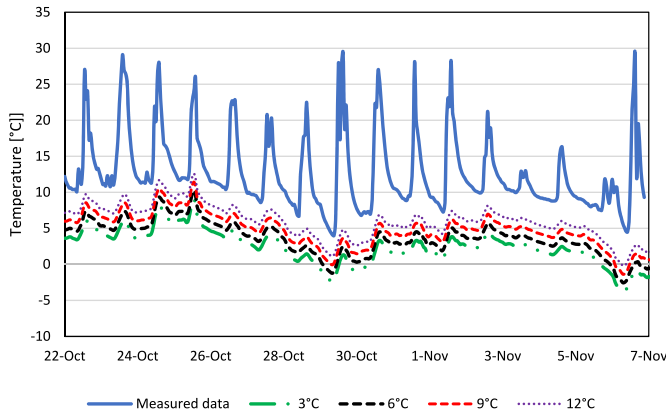


Fig. 10. Effect of soil constant temperature.

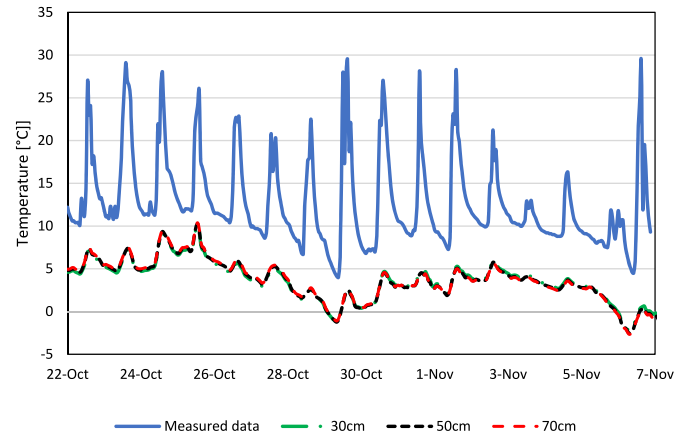


Fig. 11. Effect of thickness of soil layer.

direct paths and paths through one or multiple reflections. The diffuse solar radiation heat flux vector in an enclosed zone can be described as

$$\dot{Q}_{diffsol} = -G_{diffsol}^T A I_{diffsol} \quad (12)$$

Here,  $G_{diffsol}^T$  is the transpose of the solar Gebhart matrix,  $I_{diffsol}$  is the diffuse radiation transmitted through windows surfaces. The solar Gebhart matrix is calculated from the reflectivity  $\rho_{diffsol}$  and view factor matrix  $F$  as shown in the equation below.

$$G_{diffsol} = (I - F\rho_{diffsol})^{-1} F(I - \rho_{diffsol}) \quad (13)$$

The transient conduction thermal transfer on the inside surface is a function of the present and past values of the conduction heat flux on the inside surface temperature as described below.

$$\dot{q}_{cd,i} = \sum_{h=0}^{n_{d_s}} b_s^h T_{s,o}^h - \sum_{k=0}^{n_{e_b_s}} c_s^k T_{s,i}^k - \sum_{k=0}^{n_{d_s}} d_s^k \dot{q}_{cd,i}^k \quad (14)$$

The discrete time series coefficients  $b$ ,  $c$  and  $d$  are calculated using the z-transfer function algorithm, and the superscript  $h$  represents the term in the time series (i.e.,  $h = 0$  and  $h = 1$  refers to the current time and the past time respectively).

### 3.3. Thermal and optical transfer in windows

The model allows for the thermal and optical performance of up to 6 windowpanes to be analyzed. The temperature of each pane is determined layer-by-layer considering these physical phenomena; the transmission, absorption, and reflection of shortwave (beam and diffuse) radiation from the exterior environment, reflected diffuse radiation from surfaces in the interior environment or internal shading, the thermal transfer by convective, conductive, and radiative modes between the panes and with the interior and exterior boundaries.

In the thermal transfer analysis, the convective, conductive, and long-wave radiative heat transfer between individual panes is considered separately. The individual pane temperature is determined iteratively after the distribution of solar radiation in all the air nodes is considered and the convective and radiative heat coefficients are updated. The iterative process is performed until the change of pane temperatures gets lower than the specified tolerance. The mathematical equations describing the heat flux from the pane on the interior side to the ambient are given in (TRNSYS 18, 2021). The overall absorbed solar radiation is calculated after the individual pane temperatures are determined and distributed to the interior and exterior temperature nodes.

The optical performance is analyzed using a two-band solar radiation model which splits the shortwave radiation into visual and nonvisual parts. The front and back side visual and non-visual transmission and the absorption and reflection are calculated separately.

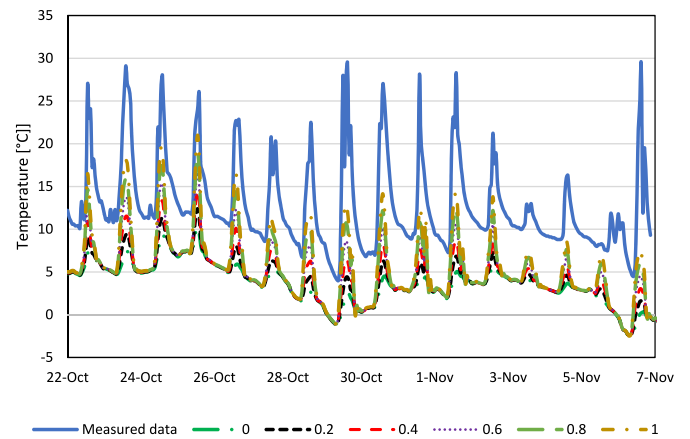


Fig. 12. Effect of solar to air fraction.

## 4. Results and discussion

### 4.1. Greenhouse ground/floor parameters

The constant soil temperature and the thickness of the soil layer with negligible temperature fluctuation effects on the model result were investigated in the section. The effect of the constant soil temperature on the temperature of the growing area is shown in Fig. 10. The measured soil temperature profile at a 50 cm depth in Olds Alberta during the calibrated period had an average of 5 °C (Alberta Climate Information Service, 2022). As the soil temperature of the perimeter of the greenhouse may be different from the recorded temperature from the weather station, we varied it from 3 °C to 12 °C in an interval of 3 °C to investigate its effect on the model. The thickness of the soil layer was set as 50 cm. The trend of the measured results and the simulation result qualitatively match. There is a deviation in the valley of the temperature profile between the measured and the simulated results for the different soil temperatures. The result shows that as the soil temperature increases, this deviation is reduced implying a significant sensitivity of the model results to the soil temperature. This is because as the soil temperature decreases, it acts as a heat sink since the thermal gradient between the indoor environment and the exterior of the ground becomes greater.

The effect of the thickness of the soil layer is shown in Fig. 11. The soil temperature is set as 6 °C and the thickness is varied from 30 cm to 70 cm in steps of 20 cm. From Fig. 11, the result shows the simulated temperature of the growing area of the greenhouse at the different thicknesses of the soil layer to lie on one another implying the model

**Table 4**  
Initial Investment and Production cost of tomatoes production in a typical greenhouse in Alberta.

Cost type	Cost item	Value (CA \$/m <sup>2</sup> )
Investment cost	Land	10.93
	Buildings	98.11
	Machinery and Equipment	20.95
Annual Capital cost	Capital Interest	0.8
	Property/Business Tax	0.27
	Depreciation of building and equipment	5.18
Annual Variable cost	Production Materials and Supplies	13.76
	Natural gas	10.82
	Other utility costs	5.07
	Labour cost	30.87
	Transportation and trucking costs	2.86
	Repairs and Maintenance costs	0.87
	Marketing charges	19.3
	Miscellaneous charges	3.53

result is insensitive to the layer thickness which may be because of the thermal gradient between the indoor environment and the ground exterior are the same for all cases.

#### 4.2. Solar-to-air factor

The result for the factor which defines the fraction of shortwave radiation entering the growing area which immediately gets converted to convective heat energy and raises the greenhouse temperature is presented. This factor is termed the solar-to-air factor, it is varied from 0 to 1 with the soil depth set to 50 cm and the constant soil temperature set to 6 °C. From Fig. 12, we observe that this factor strongly affects the daily spike and fall in the temperature profile of the growing area. As the factor is increased from 0 to 1, the deviation in the magnitude of the daily temperature rise and fall of the simulated data from the measured data is reduced. The solar-to-air factor is dependent on the presence of low-heat capacity elements in the space. The deviation of the valley of the simulated curve and measured curve may be due to the uncertainty in the constant soil temperature value used for the simulation. The model does not include the interior shading utilized at night for heat preservation purposes. Further controlled experiments need to be done to determine the solar-to-air fraction of the greenhouse interior environment.

### 5. Financial analysis

The Net Present Value (NPV) and the payback period are the estimated criteria of our financial analysis. The net present value estimates the current worth of the annual streams of net return of the investment accrued through the project lifetime. In estimating, the current worth of returns, the concept of the time value of money is applied by discounting the projected annual streams of future net returns  $NR_t$  by a specified rate termed the discount rate  $r$ . This calculation is performed for the expected lifespan of the project  $n$ , and it is expressed mathematically in Eq. (15).

$$NPV = \sum_{t=0}^n \frac{NR_t}{(1+r)^t} \quad (15)$$

The investment payback period is the time it takes from the project start for the net streams of net returns to offset the costs of the project. The length of time is calculated by setting the NPV to zero. The discount rate should be chosen to reflect the opportunity cost of capital and there are practical issues in estimating this minimum rate of new investment returns. Most countries think the rate lies between 8% and 15% and most analyses are performed using 12% (James, 1972). Most agricultural projects are not expected to become obsolete within a twenty- and twenty-five-year period due to technological advancement (James, 1972). For our analysis, the discount factor and project lifespan are set to

**Table 5**  
Financial analysis results.

	Net Present Value (CA \$/m <sup>2</sup> )	Payback Period (years)
Typical greenhouse	581.03	652.75
Passive solar greenhouse	1.47	1.39

12% and 15 years respectively.

#### 5.1. Cost and benefits of tomatoes production in a greenhouse

The different benefits and costs of agricultural greenhouse production need to be identified and valued at monetary prices to perform a financial analysis of the agricultural projects. For our analysis, the production cost is comprised of the capital investment cost, capital costs and variable costs. The capital investment cost is the initial expense for the purchase of physical assets required for the greenhouse operation which includes the land cost, building cost and machinery and equipment costs. The capital costs are the operational cost that stays fixed independent of the greenhouse production level, such costs include the depreciation cost of building and equipment, property taxes and interest on capital. The variable costs are operational costs that depend on the production level of the greenhouse and include material input costs, labour costs, cost of maintenance and repairs, heating costs, transportation costs, marketing costs and other miscellaneous expenses. The reference greenhouse grows tomatoes, cucumbers, peppers, and cabbage but for simplicity, the financial analysis presented is based on the production of tomatoes. The identified costs for the greenhouse operation are summarized in Table 4, the monetary values of this cost are based on results from a survey of commercial greenhouse producers conducted by the Alberta Agricultural and Rural Development Authority in 2017 (Laate, 2018).

In 2017, the greenhouse area for tomato production in Alberta was about 212,860 m<sup>2</sup> and the survey data was reported based on results from seven producers with a greenhouse area of 7186 m<sup>2</sup>. The depreciation value in Table 4 was calculated using the straight-line method as shown in Eq. (16) with a salvage value of 10% of the purchase price. The life span of the buildings, machinery and equipment were estimated by the participating greenhouse producers.

$$\text{Depreciation} = \frac{\text{Purchase Price} - \text{Salvage Value}}{\text{Life span}} \quad (16)$$

The residual value of the building and equipment is treated as a benefit at the end of the project and for equipment with a lifespan shorter than the project lifespan, a replacement cost is added once the equipment becomes obsolete.

The natural gas cost represents the heating cost of the greenhouse and for the reference greenhouse that operates with no heating cost, this value is set to zero in the analysis. Based on the total greenhouse area, the application of the reference greenhouse across the province of Alberta for tomato production can result in annual heating cost savings of about CA\$ 2.3 million. The reference greenhouse construction was done almost entirely by the greenhouse producer with materials imported from China, estimating the cost is complex, so we assume it cost the same amount as the average greenhouse and a sensitivity analysis of the implication of the changes in this price is presented in Section 5.3.

The measure of benefits in our financial analysis is the gross return value of crops produced in the greenhouse. The average return of the surveyed tomato-producing greenhouses in Alberta in 2017 was CA\$ 94.16 per m<sup>2</sup>. This value is significantly less compared to the value computed based on attainable target yields of greenhouse in Alberta and the price of tomatoes in November 2018. For new growers of tomatoes, the attainable yield is between 50 and 55 kg/m<sup>2</sup> with the more experienced growers attaining yields over 60 kg/m<sup>2</sup> of the production area (Calpas, 2023). The market price of tomatoes in Alberta was C\$ 4.01/kg.

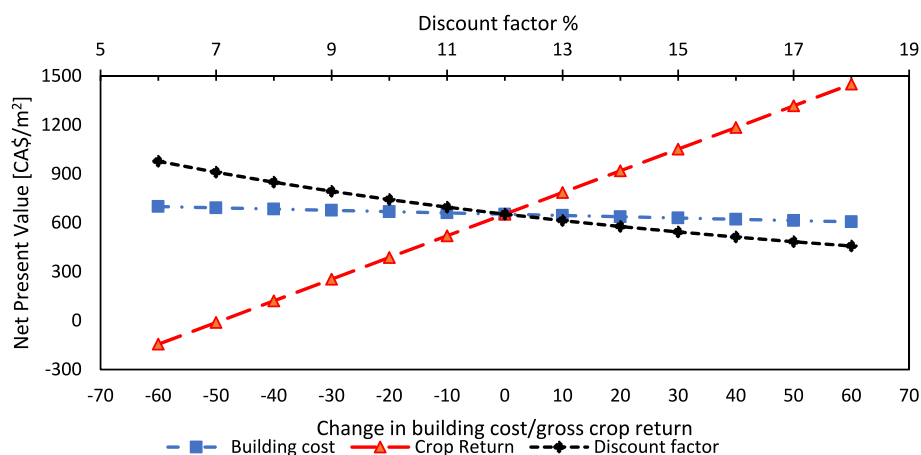


Fig. 13. Sensitivity analysis of NPV to changes in building cost, gross return and discount factor.

in October 2019 (Government of Alberta, 2019) which gives a return of CA\$ 200.5 per m<sup>2</sup>. Although the market price is higher than the farm gate price, a return of CA\$ 200.5 per m<sup>2</sup> is assumed and the impact of this variable is analyzed in the sensitivity study presented in Section 5.3.

### 5.2. Financial analysis result

The financial analysis result computed is computed for the reference CSG and a typical greenhouse in Alberta. The calculations are based on an economic lifespan of 15 years for the tomatoes-producing greenhouse, a discount rate of 12% and the retail price of tomatoes. The result is summarized in Table 5. The NPV for tomato production in the typical greenhouse and passive CSG are CA\$ 581.03 /m<sup>2</sup> and CA\$ 652.75 / m<sup>2</sup> with a payback period of 1.47 yrs and 1.39 yrs respectively. The NPV greater than zero and the payback period less than the lifespan shows the project is financially viable. The monetary value assigned to parameters like the cost of the reference passive solar greenhouse, the greenhouse production crop yield and the discount factor are faced with uncertainty. To understand the implication of changes in these parameters, a one-parameter-at-a-time sensitivity analysis is performed. Comparing our findings to a similar feasibility study performed with the greenhouse location in Saskatchewan (Ahamed et al., 2019), they found the NPV to be CA\$ 1.9 million (CA\$ 320 /m<sup>2</sup>) with a payback period was 2.42 yrs. The value is comparable to our finding and the difference can be linked to the supplementary requirement for heating, a shorter estimated life span and a lower discount factor used in their estimate.

### 5.3. Sensitivity analysis

The analysis for the reference building is reworked adjusting the cost of the building, gross return value of crop produced and the discount factor one at a time to determine how sensitive the NPV is to these parameters. The building cost and gross return are adjusted six intervals above and below the initial value in steps of 10% while values of discount factor ranging from 6% to 18% in steps of 1% are used for the sensitivity analysis. The result of this sensitivity analysis is presented in Fig. 13 and it shows the estimated NPV to be most sensitive to the gross return value of the crop and least sensitive to changes in building cost. The results show that if the reference CSG is 60% cheaper than the typical greenhouse, the NPV increases by 7% and if it is 60% more expensive, the NPV decreases by 7%. Adjusting the discount rate from 6% to 18% changes the NPV from CA\$ 977.16 /m<sup>2</sup> to CA\$ 457.53 / m<sup>2</sup>. The sensitivity result for the changes in gross crop return gives a negative net present worth when the gross return is reduced by 60% implying

the production is not feasible at this gross crop return rate.

## 6. Conclusion

In this study, the numerical modelling of a net-zero Chinese-style greenhouse in Alberta using TRNSYS is presented. The simulated indoor temperature profile qualitatively matches the measured temperature results. The effects of the ground parameters and the solar-to-air factor were investigated. The simulation result shows the numerical model to be sensitive to the ground temperature and the solar-to-air fraction. The simulated indoor temperature profile decreases as the ground temperature decrease. The result shows the solar-to-air factor to be the factor responsible for the daily spike in indoor temperature. Further controlled indoor climate monitoring and measurement are required for proper calibration of this parameter.

The result of the financial analysis using tomato production as a case study shows the reference CSG to be more economically viable than the traditional greenhouse. The retail price of tomatoes production was used for this analysis and the sensitivity study shows the NPV to be sensitive to this parameter.

### CRediT authorship contribution statement

**Oselen J. Imafidon:** Conceptualization, Methodology, Software, Formal analysis, Visualization, Writing – original draft. **David S-K. Ting:** Resources, Writing – review & editing, Supervision. **Rupp Cariveau:** Resources, Writing – review & editing, Supervision.

### Declaration of competing interest

The authors declare that they have no known competing financial interests or personal relationships that could have appeared to influence the work reported in this paper.

### Data availability

Data will be made available on request.

### Acknowledgement

The authors are grateful to Jianyi Dong of Freshpal Farms, Alberta for sharing the greenhouse data.

## References

- 1728 Software Systems, 2001. Dew point calculator At: [https://www.1728.org/dewp\\_oimt.htm](https://www.1728.org/dewp_oimt.htm) (Accessed 29 December, 2022).
- Ahamed, Md S., Guo, H., Tanino, K., 2018. Development of a thermal model for simulation of supplemental heating requirements in Chinese-style solar greenhouses. *Comput. Electron. Agric.* 150, 235–244. <https://doi.org/10.1016/j.compag.2018.04.025>.
- Ahamed, M.S., Guo, H., Taylor, L., Tanino, K., 2019. Heating demand and economic feasibility analysis for year-round vegetable production in Canadian Prairies greenhouses. *Information Processing in Agriculture* 6 (1), 81–90. <https://doi.org/10.1016/j.inpa.2018.08.005>.
- Alberta Climate Information Service, 2022. Current and Historical Alberta Weather Station Data Viewer. At: <https://acis.alberta.ca/weather-data-viewer.jsp>.
- Aschaber, J., Hiller, M., Weber, R., 2009. Trnsys17: new features of the multizone building model. In: 11th International Building Performance Simulation Association Conference, Glasgow, Scotland.
- Beshada, E., Zhang, Q., Boris, R., 2006. Winter performance of a solar energy greenhouse in southern Manitoba. *Can. Biosyst. Eng.* 48 (5), 1–8.
- Britannica, 2019. Canada - Climate. Encyclopædia Britannica [Online]. Available: <http://www.britannica.com/place/Canada/Climate>. (Accessed 15 January 2023).
- Calpas, J., 2023. Commercial greenhouse tomato production. At: <https://www.alberta.ca/commercial-greenhouse-tomato-production.aspx>. (Accessed 9 May 2023).
- Cao, K., et al., 2019. Renewable and sustainable strategies for improving the thermal environment of Chinese solar greenhouses. *Energy Build.* 202, 109414. <https://doi.org/10.1016/j.enbuild.2019.109414>.
- Cuce, E., Harjunowibowo, D., Cuce, P.M., 2016. Renewable and sustainable energy saving strategies for greenhouse systems: a comprehensive review. *Renew. Sustain. Energy Rev.* 64, 34–59. <https://doi.org/10.1016/j.rser.2016.05.077>.
- Dias, G.M., Ayer, N.W., Khosla, S., V Acker d, R., Young, S.B., Whitney, S., Hendricks, P., 2017. Life cycle perspectives on the sustainability of Ontario greenhouse tomato production: benchmarking and improvement opportunities. *J. Clean. Prod.* 140, 831–839. <https://doi.org/10.1016/j.jclepro.2016.06.039>.
- Dong, S., Ahamed, S., Ma, C.-W., Guo, H., 2021. A time-dependent model for predicting thermal environment of mono-slope solar greenhouses in cold regions. *Energies* 14 (18), 5956. <https://doi.org/10.3390/en14185956>, 5956.
- Energyhub, 2019. Solar Power Alberta (Complete Guide 2021). At: <https://www.energyhub.org/alberta/>. (Accessed 16 May 2023).
- Gao, L.-H., Qu, M., Ren, H.-Z., Sui, X.-L., Chen, Q.-Y., Zhang, Z.-X., 2010. Structure, function, application, and ecological benefit of a single-slope, energy-efficient solar greenhouse in China. *HortTechnology* 20 (3), 626–631. <https://doi.org/10.21273/horttech.20.3.626>.
- Government of Alberta, 2019. Edmonton Retail Food Prices Food Items by Category. At: <https://open.alberta.ca/dataset/64171713-56dc-488d-bcdf-9b85f4833a2c/resource/b115237a-c41e-472c-a9c5-48fa4a9a314c/download/af-edmonton-retail-food-prices-average-monthly-2019-11.pdf>. (Accessed 18 May 2023).
- Henshaw, P., 2017. Modelling changes to an unheated greenhouse in the Canadian subarctic to lengthen the growing season. *Sustain. Energy Technol. Assessments* 24, 31–38. <https://doi.org/10.1016/j.seta.2016.12.004>.
- IESO, 2019. New study shows energy cost savings potential for Ontario greenhouses. At: [www.ieso.ca](http://www.ieso.ca) <https://www.ieso.ca/en/Corporate-IESO/Media/News-Releases/2019/10/New-Greenhouse-Study> (Accessed Jan 17, 2023).
- James, P., 1972. *Gittinger Economic Analysis of Agricultural Projects*. Johns Hopkins University Press, Baltimore.
- Kalogirou, S.A., Florides, G.A., 2004. Measurements of Ground Temperature at Various Depths in 3rd International Conference on Sustainable Energy Technologies, 2004 (Nottingham, UK).
- Laate, E.A., 2018. Economics of production and marketing greenhouse crops in Alberta. *Edmonton Alberta agriculture and Forestry*. At: <https://open.alberta.ca/data-set/fbb2b0b5-53b9-4dbd-92b7-f37ec8ed9369/resource/d074794d-7ec0-4bef-bc93-99a57bbc2cf2/download/2017greenhousecop.pdf>. (Accessed 5 May 2023).
- Labby, B., 2021. A Former Geologist Imports a Popular Chinese Model to Grow Veggies Year-Round in Alberta's Harsh Climate. CBC [Online]. Available: <https://www.cbc.ca/news/canada/calgary/passive-solar-greenhouse-alberta-1.6289155>. (Accessed 16 January 2023).
- Liu, X., Li, Y., Liu, A., Yue, X., Li, T., 2019. Effect of North wall materials on the thermal environment in Chinese solar greenhouse (Part A: experimental researches). *Open Phys.* 17 (1), 752–767. <https://doi.org/10.1515/phys-2019-0079>.
- Liu, X., Li, H., Li, Y., Yue, X., Tian, S., Li, T., 2020. Effect of internal surface structure of the north wall on Chinese solar greenhouse thermal microclimate based on computational fluid dynamics. *PLoS One* 15 (4), e0231316. <https://doi.org/10.1371/journal.pone.0231316>.
- Mazzeo, D., Baglivo, C., Panico, S., Congedo, P.M., 2021. Solar greenhouses: climates, glass selection, and plant well-being. *Sol. Energy* 230, 222–241. <https://doi.org/10.1016/j.solener.2021.10.031>.
- Natural Resource Canada, 2016. Photovoltaic potential and solar resource maps of Canada. At: <https://open.canada.ca/data/en/dataset/8b434ac7-aedb-4698-90df-ba77424a551f>. (Accessed 10 May 2023).
- Rasheed, A., Lee, J.W., Lee, H.W., 2018. Development of a model to calculate the overall heat transfer coefficient of greenhouse covers. *Spanish J. Agric. Res.* 15 (4), e0208 <https://doi.org/10.5424/sjar/2017154-10777>.
- Tong, G., Christopher, D.M., Li, T., Wang, T., 2013. Passive solar energy utilization: a review of cross-section building parameter selection for Chinese solar greenhouses. *Renew. Sustain. Energy Rev.* 26, 540–548. <https://doi.org/10.1016/j.rser.2013.06.026>.
- TRNSYS 18, 2021. *Multizone Building Modelling with Type 56 and TRNBuild*, 5. Solar Energy Laboratory, University of Wisconsin, Madison, WI.
- TRNSYS-users Archives, 2023. At: <http://lists.onebuilding.org/pipermail/trnsys-users-onebuilding.org/> (Accessed January, 16, 2023).
- Wang, J., Li, S., Guo, S., Ma, C., Wang, J., Jin, S., 2014. Simulation and optimization of solar greenhouses in northern jiangsu province of China. *Energy Build.* 78, 143–152. <https://doi.org/10.1016/j.enbuild.2014.04.006>.
- Zhang, Y., Zou, Z.R., 2013. Structure and properties of solar-greenhouse with variable incidence angle. *Journal of Northwest A & F University - Natural Science Edition* 41 (11), 113–118.
- Zhang, Y., Bao, C., Cao, Y., 2011. Analysis on measurement of heat absorption and release of wall and ground in two different solar greenhouses. *Res Agric Mod* 32 (4), 509–512 (in Chinese with English abstract).

## Glossary

## Alphabetical Symbols

- A: Diagonal matrix of internal surface area in an enclosed zone ( $m^2$ )
- $Abs_1$ : Solar absorptance of glazing system layer 1 at each incidence angle (–)
- $Abs_2$ : Solar absorptance of glazing system layer 2 at each incidence angle (–)
- $a_s, b_s, c_s$  and  $d_s$ : Conduction transfer functions coefficients (–)
- F: View factor matrix (–)
- $F_{sky}$ : View factor with the sky (–)
- $f_{solar}$ : Solar-to-air factor (–)
- $G_b$ : Beam solar radiation on the external surface ( $W/m^2$ )
- $G_d$ : Diffuse radiation on the external surface ( $W/m^2$ )
- $G_r$ : Reflected radiation on the external surface ( $W/m^2$ )
- $G_{lw}$ : Gebhart matrix for longwave radiation (–)
- $G_{lw}^T$ : Transpose of the Gebhart matrix (–)
- $G_{diffsol}$ : Solar Gebhart matrix (–)
- $G_{diffsol}^T$ : Transpose of the solar Gebhart matrix (–)
- Hem: Value integrated over the hemisphere
- $h_i$ : Interior surface heat transfer coefficient ( $W/m^2K$ )
- $h_o$ : Exterior surface heat transfer coefficient ( $W/m^2K$ )
- I: Identity matrix (–)
- $I_{diffsol}$ : Diffuse radiation transmitted through windows surfaces ( $W/m^2$ )
- n: Expected Lifespan of project (years)
- NPV: Net Present Value ( $CAS/m^2$ )
- NR<sub>t</sub>: Net return at year t ( $CAS/m^2$ )
- $\dot{q}_{cd,i}$ : Conduction heat flux at the interior surface ( $W/m^2$ )
- $\dot{q}_{cd,o}$ : Conduction heat flux at the exterior surface ( $W/m^2$ )
- $\dot{q}_{cv,i}$ : Convective heat flux from the interior side to the zone air ( $W/m^2$ )
- $\dot{q}_{cv,o}$ : Convective heat flux between the exterior side and its surrounding environment ( $W/m^2$ )
- $\dot{Q}_{diffsol}$ : Diffuse solar radiation heat flux vector in an enclosed zone (W)
- $\dot{q}_{lw,i}$ : Net infrared radiation with the surfaces within the zone ( $W/m^2$ )
- $\dot{q}_{lw,o}$ : Infrared radiation exchange between the exterior side and objects within its view ( $W/m^2$ )
- $\dot{Q}_{lw}$ : Net infrared radiation matrix (W)
- $\dot{q}_{sol,i}$ : Solar radiation transmitted through windows absorbed at the internal surface ( $W/m^2$ )
- $\dot{q}_{sol,o}$ : Shortwave radiation absorbed by the exterior side ( $W/m^2$ )
- r: Discount factor (%)
- $R_{bsol}$ : Back surface solar reflectance of the glazing system at each incidence angle (–)
- $R_{fsol}$ : Front surface solar reflectance of the glazing system at each incidence angle (–)
- RH: Relative humidity (–)
- t: Project year (year)
- T: Surface temperature vector (K)
- $T_{amb}$ : Ambient temperature (K)
- $T_{dp}$ : Dewpoint temperature (K)
- $T_{ext}$ : Exterior environment temperature (K)
- $T_{fsky}$ : Fictitious sky temperature (K)
- $T_{grad}$ : Weighted temperature of the ground (K)
- $T_{sol}$ : Solar transmittance of the glazing system (–)
- $T_{sky}$ : Weighted temperature of the sky (K)
- $T_{s,i}$ : Interior surface temperature (K)
- $T_{s,o}$ : Outer surface temperature (K)
- $T_{vis}$ : Visible light transmission of the glazing system at each incidence angle (–)
- $T_{zone}$ : Temperature of zone (K)

## Greek Symbols

- $\alpha_{sol,o}$ : Solar absorptivity of the outer surface
- $\epsilon_{s,o}$ : Emissivity to infrared radiation of exterior surface (–)
- $\epsilon_{lw}$ : Emissivity to longwave radiation (–)
- $\rho_{lw}$ : Reflectivity to longwave radiation (–)
- $\rho_{diffsol}$ : Reflectivity to solar radiation (–)
- $\sigma$ : Stefan Boltzmann constant ( $W/m^2K^4$ )